Role of degassing of the Noril'sk nickel deposits in the Permian–Triassic mass extinction event

Margaux Le Vaillant[a,1], **Stephen J. Barnes**[a], **James E. Mungall**[b], **and Emma L. Mungall**[c]

[a]Commonwealth Scientific and Industrial Research Organisation, Mineral Resources, Kensington, WA 6151 Australia; [b]Department of Earth Sciences, University of Toronto, Toronto, ON M5S 3B1, Canada; and [c]Department of Chemistry, University of Toronto, Toronto, ON M5S 3H6, Canada

Edited by Charles H. Langmuir, Harvard University, Cambridge, MA, and approved January 13, 2017 (received for review July 7, 2016)

The largest mass extinction event in Earth's history marks the boundary between the Permian and Triassic Periods at circa 252 Ma and has been linked with the eruption of the basaltic Siberian Traps large igneous province (SLIP). One of the kill mechanisms that has been suggested is a biogenic methane burst triggered by the release of vast amounts of nickel into the atmosphere. A proposed Ni source lies within the huge Noril'sk nickel ore deposits, which formed in magmatic conduits widely believed to have fed the eruption of the SLIP basalts. However, nickel is a nonvolatile element, assumed to be largely sequestered at depth in dense sulfide liquids that formed the orebodies, preventing its release into the atmosphere and oceans. Flotation of sulfide liquid droplets by surface attachment to gas bubbles has been suggested as a mechanism to overcome this problem and allow introduction of Ni into the atmosphere during eruption of the SLIP lavas. Here we use 2D and 3D X-ray imagery on Noril'sk nickel sulfide, combined with simple thermodynamic models, to show that the Noril'sk ores were degassing while they were forming. Consequent "bubble riding" by sulfide droplets, followed by degassing of the shallow, sulfide-saturated, and exceptionally volatile and Cl-rich SLIP lavas, permitted a massive release of nickel-rich volcanic gas and subsequent global dispersal of nickel released from this gas as aerosol particles.

Noril'sk Ni–Cu–PGE deposits | Permian–Triassic mass extinction | sulfide flotation

The record of the extinction in the Permian–Triassic (P-Tr)-type section at Meishan, China (1) shows that the event occurred between the deposition of two ash beds that yielded U–Pb zircon chemical abrasion isotope dilution–thermal ionization mass spectrometry ages of 251.941 ± 0.037 and 251.880 ± 0.031 Ma (1). The Siberian Trap large igneous province (SLIP) is the world's most voluminous subaerial igneous province, covering 1.5×10^6 km^2 with an estimated volume of 4×10^6 km^3 (2). SLIP activity was reported to have lasted ~300 ky, before and concurrent with the P-Tr mass extinction, and continuing for at least 500 ky after extinction cessation (3). This age model agrees with the magmatism of the SLIP representing a trigger for the P-Tr mass extinction; within this time span there is a clear temporal link between the emplacement of NiS ore-bearing intrusions in the SLIP, starting at 251.907 ± 0.094 Ma, and the onset of extinction (3).

The extinction interval in the Meishan sedimentary section immediately follows a sudden increase in Ni concentrations, accompanied by a catastrophic decline in δ^{13}C which peaked exactly at the base of the extinction interval. This sharply declining δ^{13}C has been linked to superexponential increase in the concentration of inorganic C in the ocean and atmosphere (4), because benthic marine colonies of the *Archaea methanosarcina* acquired a new metabolic pathway by gene transfer from a bacterium, using Ni-based enzymes to convert acetate to methane (4). This newfound capability, in the presence of a superabundance of Ni, allowed the rapid metabolism of a large global marine reservoir of shallowly buried organic carbon and led to a superexponential growth of marine and atmospheric inorganic carbon (4), leading to catastrophic mass extinction.

Nickel is a nonvolatile, strongly compatible element, normally locked up in early crystallizing silicate phases or sulfide liquid accumulations in deeper portions of subvolcanic magmatic systems and therefore tends not to be notably enriched in volcanic gases (5). However, if dissolved in volcanic gas, Ni is rapidly precipitated during cooling, forming solid aerosol particles as sulfide, oxide, or chloride phases (6). Atmospheric particulate matter is most likely to be transported far from its point of origin if its size falls within the accumulation mode (i.e., particles with a diameter of roughly 0.1–1 μm), particularly if it has limited hygroscopicity and is thus unlikely to nucleate cloud droplets (7). Observations in the plumes of both actively erupting and quiescent degassing volcanoes have shown emissions of such aerosols (8–10), and a few studies have quantified trace metals in these aerosols, observing not only large enrichments compared with background, but also large absolute concentrations of Ni and Cu in the airborne particulate phase (up to 1–2 μg m^{-3} of Cu and Ni in volcanic plumes) (5, 11–13). In particular, up to 1.6 μg m^{-3} Ni were reported to be emitted from Kilauea (14), with the large majority of that mass being present in the accumulation mode. These modern observations clearly show that Ni can be emitted in a form that allows it to be transported long distances in the atmosphere, such that it can be deposited far from its point of origin. Aerosols emitted by actively erupting volatile-rich arc volcanoes like Stromboli (5), Soufriere (11), and Merapi (6) are typically more highly enriched in Ni-bearing aerosols, having published emanation coefficients as high as 1.3%, than modern volatile-poor tholeiitic basalts [Kilauea and Eyjafjallajokull (6, 14, 15)] that typically emit relatively little Ni. The Hawaiian and Icelandic tholeiitic basalts are the modern equivalent of the SLIP lavas, raising the question of how the large masses of Ni demanded by the hypothesis of runaway marine methanogenesis could have become dispersed into the atmosphere

Significance

The Noril'sk deposits represent one of the most valuable metal concentrations on Earth and are associated with the world's largest outpouring of mafic magma. Mass release of nickel into the atmosphere during ore formation has been postulated as one of the triggers for the Permian–Triassic Mass Extinction Event, by promoting the activity of the marine *Archaea methanosarcina* with catastrophic greenhouse climatic effects. The missing link has been understanding how nickel, normally retained at depth in magmatic minerals, could have been mobilized into magmatic gases. The flotation of magmatic sulfides to the surface by gas bubbles was suggested as a possible mechanism. Here, we provide evidence of physically attached nickel-rich sulfide droplets and former gas bubbles, frozen into the Noril'sk ores.

Author contributions: M.L.V. and S.J.B. designed research; M.L.V., S.J.B., and J.E.M. performed research; M.L.V. analyzed data; J.E.M. performed partition coefficient calculations; E.L.M. performed literature review on gas and aerosols emissions; and M.L.V. wrote the paper with input from S.J.B., J.E.M., and E.L.M.

The authors declare no conflict of interest.

This article is a PNAS Direct Submission.

[1] To whom correspondence should be addressed. Email: margaux.levaillant@csiro.au.

www.pnas.org/cgi/doi/10.1073/pnas.1611086114

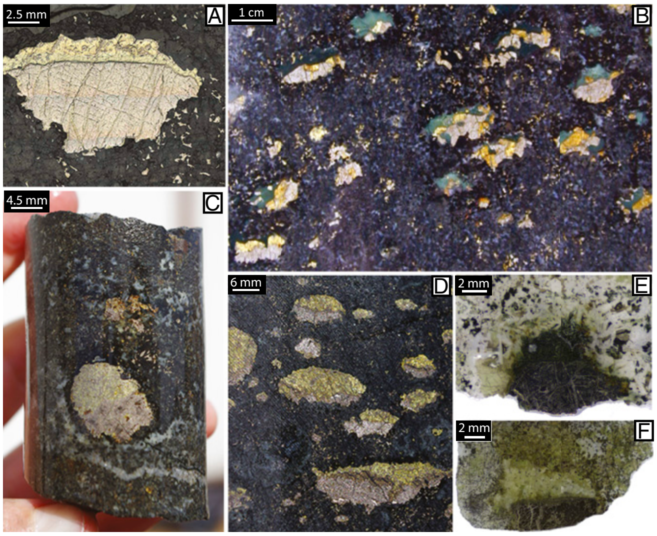

Fig. 1. Representative photographs of capped globules from the Noril'sk magmatic Ni–Cu–PGE deposits. (*A*) Sample VZU-9B from the Ni–Cu–PGE globular sulfides within the Kharaelakh intrusion. (*B*) Photograph of a sample of globular ore from the Oktyabrysk deposit, courtesy of Peter Lightfoot. (*C* and *D*) Photos of drill core samples, respectively, from drill hole OUG-2 (Talnakh deposit) and from drill hole RT-7 (Oktyabrysk deposit). (*E*) Sample NOR1-4a and (*F*) Sample NOR1-3a, both from the globular ore of the Noril'sk I deposit.

during the voluminous Siberian Trap eruptions. We suggest that a unique combination of characteristics of the SLIP permitted exceptionally large volcanic Ni aerosol emissions. (*i*) Extensive contamination of the magma by assimilation of volatile-rich evaporites allowed the production of extremely large amounts of sulfide melt, which scavenges Ni from the magma. (*ii*) A proportion of this Ni present in the sulfide melt was then transferred into the magmatic vapor phase through close physical interaction between sulfide melt and vapor bubbles. This interaction, which occurred within the subvolcanic intrusions that host the orebodies, was made possible by their shallow depth, as described in this contribution. Finally, (*iii*) eruption of volatile-enriched lavas released the Ni-enriched volcanic gas, producing Ni-enriched aerosols.

Capped Globular Sulfides

The Noril'sk nickel deposits occur within small ski-shaped subvolcanic intrusions, up to 360 m thick and 25 km long, which contain 1.7 billion tons of ore at an average grade of 0.9% Ni (16). The orebodies contain an abundance of highly distinctive globular sulfide ore textures (Fig. 1), predominantly found within the olivine cumulates that form the lower layers of the intrusions (17). We note the occurrence of a particularly interesting variant of this globular ore type we refer to as "capped globules." We interpret these capped globules as being the remnants of sulfide melt and vapor bubbles compounds now frozen in place, as shown by the following description.

These capped globules are composed of two main components, a sulfide globule and a silica cap, which together occupy a void in the otherwise continuous 3D framework of touching cumulate silicate crystals, or primocrysts, which were the first mineral phase to crystallize and accumulate in the intrusion as a layer of crystals bathed in interstitial silicate melt. The sulfide globules preferentially occupy the bottoms of the subspherical voids among the primocrysts. The globules represent the original immiscible sulfide liquid droplets that subsequently crystallized to form differentiated globules with Fe–Ni-rich pyrrhotite–pentlandite lower parts and Fe–Cu-rich chalcopyrite–cubanite upper parts (18) (Fig. 1). The upper parts of the voids, here defined as "silica caps," are in contact with the Cu-rich portion of the sulfide globules and are composed of late-crystallizing silicate minerals. The composition of these late-crystallizing minerals is similar to that of the minerals forming in the interstitial space between the early-formed cumulate primocrysts. We have imaged capped globules using both 2D micro-X-ray fluorescence (micro-XRF) imaging of thin sections (Fig. 2), and 3D micro X-ray computed tomography (3D micro X-ray CT, Fig. 3). We observe capped globules independently of the nature of the primocryst framework: olivine, plagioclase, or even chromite (Fig. 2).

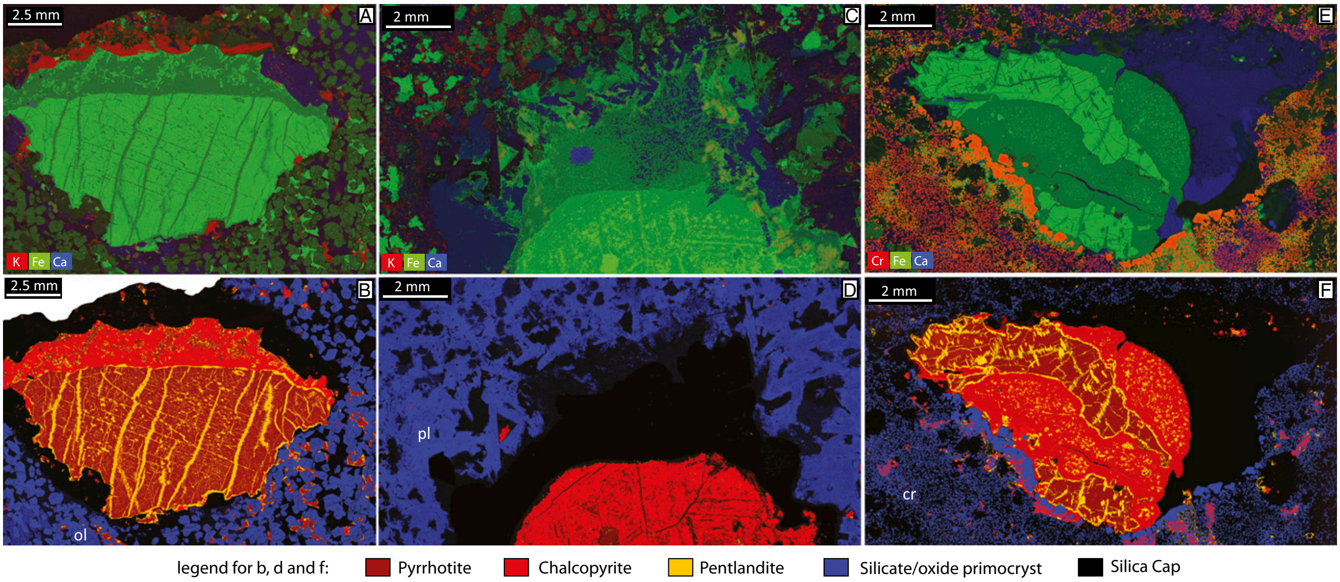

Fig. 2. Three elemental maps (*A*, *C*, and *E*) and phase maps (*B*, *D*, and *F*) of capped globules from the globular ore from the Karaelakh (*A* and *B*), the Noril'sk (*C* and *D*) and the Talnakh (*E* and *F*) intrusions. The three-elemental maps were produced using the data collected with the Maia detector array on the XRF microscopy beamline, at the Australian Synchrotron in Melbourne, Australia. ol, olivine; pl, plagioclase; cr, chromite.

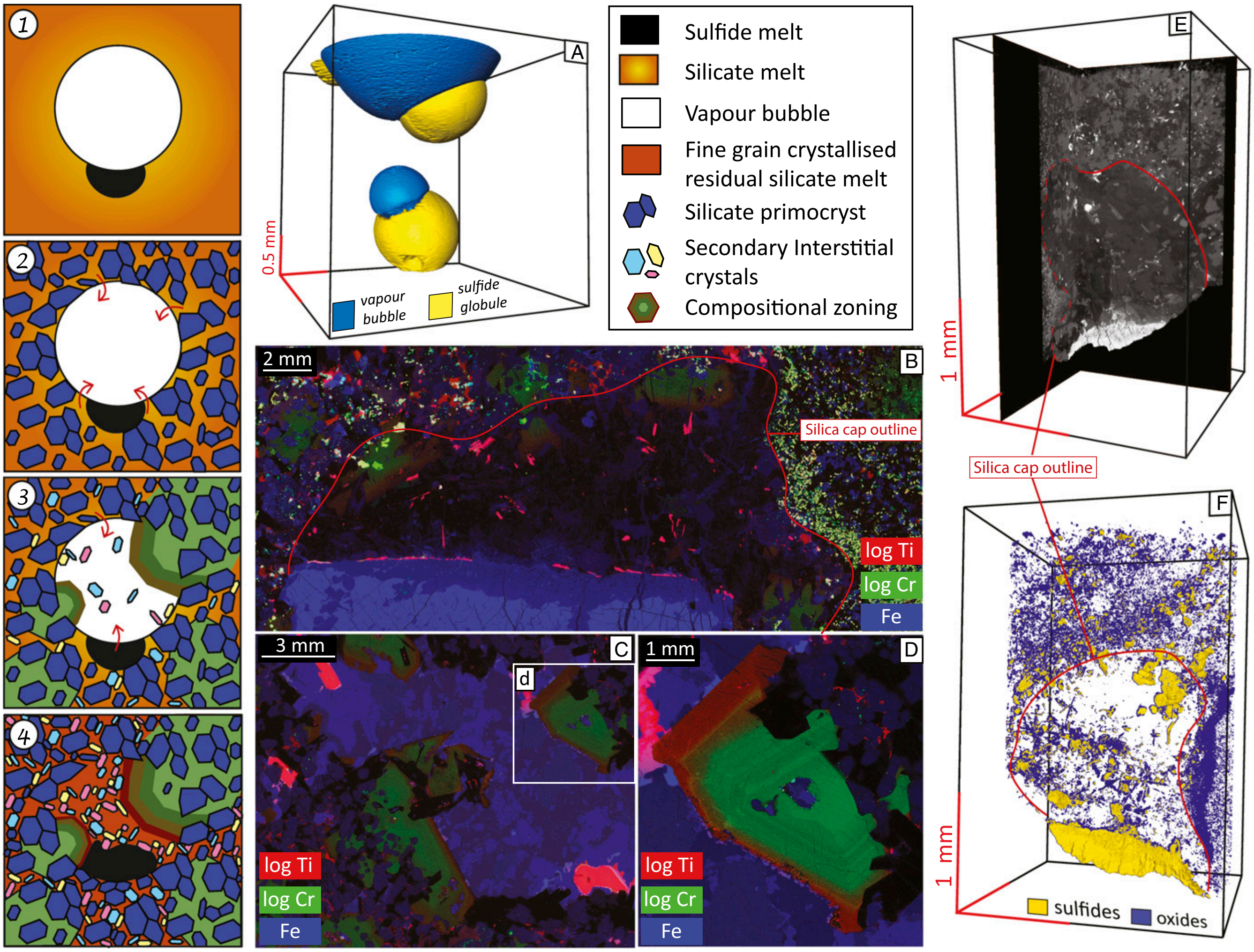

Fig. 3. Sequences 1–4 show the evolution of the compound sulfide globules and attached vapor bubble (step 1) during crystallization of the magma chamber. First the primocrysts crystallize and form a close-packed solid framework that holds existing vapor bubbles and sulfide globules fixed in place (step 2). Then the residual melt slowly crystallizes, more small vapor bubbles form in the intercumulus space and force residual melt to partially fill in the vapor bubble (step 3), which is forced to shrink by the increasing intercumulus pore fluid pressure, and in the final stage, some of the sulfide melt itself gets pushed into the last void space and crystallizes (step 4). (*A*) Three-dimensional segmentation of a micro-CT analysis of an experimental run showing compound sulfide bleb attached to vapor bubbles; data from ref. 19. Blue represents the vapor bubble and the sulfide globules are in yellow. (*B*–*D*) Three-elemental maps showing compositional zoning of clinopyroxenes growing within the void left by the presence of the vapor bubble attached to the sulfide globule. These maps were produced using the data collected with the Maia detector array on the XRF microscopy beamline, at the Australian Synchrotron in Melbourne. *E* and *F* were produced using data from high-resolution X-ray CT (HRXCT) 3D analysis of sample NOR1-3a. (*E*) Gray-scale image in two directions representing projections on the entire HRXCT dataset along *X* and *Y* directions. (*F*) Three-dimensional volume rendering of sulfide and oxide phases within the sample. In this sample, primocrysts are chromite (one type of oxide), which grow around the vapor bubble. Within this micro-CT dataset, chromite and other oxides that crystallized later could not be distinguished, so they were modeled together, hence the presence of some oxide crystals where the vapor bubble used to sit. In images *B*, *E*, and *F*, the red line represents the outline of the silica cap.

Typically the silica caps are filled with strongly differentiated, late-crystallizing magmatic silicate minerals such as plagioclase, clinopyroxene, orthopyroxene, and titanite as well as Ti-rich magnetite, ilmenite, and Cl-rich apatite. In many cases, volatile-containing silicate phases, particularly amphiboles, micas, and chlorite (clinochlore), are also present. Faceted morphologies and concentric growth zoning defined by Cr and Ti abundances (Fig. 3 *B*–*D*) are observed in clinopyroxene and oxides growing in the silica caps. These characteristics are strongly suggestive of free growth of these pyroxenes and oxides into pockets of crystal-free melt (Fig. 3). In some cases carbonate minerals and anhydrite are also present in the center of the caps, leading to the interpretation that at least part of each silica cap is an amygdule (amygdules are originally open spaces in volcanic or very shallow intrusive rocks left behind by magmatic vapor bubbles that have subsequently been filled in by low-temperature minerals).

We interpret the voids in the primocryst frameworks as the result of the presence of vapor bubbles attached to the sulfide liquid at the time of crystallization of the primocrysts (Fig. 3, steps 1 and 2). Recent published observations provide an essential clue to the processes in operation. Where sulfide melt, silicate melt, and vapor bubbles coexist, vapor bubbles have a strong tendency to nucleate against and remain attached to sulfide droplets owing to surface tension effects (19) (Fig. 3*A*).

We interpret the silicate caps as the result of fractionated interstitial silicate melt being driven into residual porosity during late stages of solidification and crystal overgrowth of the primocrysts by the gas-filter pressing mechanism (20), which has also been invoked to explain the occurrence of segregation vesicles in basalts. In this mechanism, crystallization of the intercumulus residual melt causes nucleation and growth of numerous smaller vapor bubbles. The increase in intercumulus fluid pressure leads to strong pressure gradients that cause progressive infilling by residual silicate melt of the original large vapor bubbles residing in the void space. In this way, the original vapor bubbles fill with highly differentiated interstitial liquid to accommodate the growth of many smaller bubbles in the intercumulus spaces, giving rise to strong zoning from Cr-rich to Cr-poor, Ti-rich phases within the silica caps (Fig. 3). The same process drives some of the sulfide liquid into the intercumulus space surrounding the original compound bubble and drop (Fig. 3, steps 3 and 4).

The capped globules described here record the close spatial and genetic association between magmatic vapor and Ni-rich sulfide droplets (19). Depending on the proportion of the phases (liquid sulfides and vapor), this association with vapor bubbles may enable sulfide droplets to float within a much less dense mafic magma like a basket beneath a hot-air balloon. On this basis, we suggest that the Noril'sk capped globules may have been transported and deposited as composite droplet–bubble pairs by a vapor-saturated magma (Fig. 4).

Although the only preserved examples of this association between sulfide globules and vapor bubbles now occur within the cumulate layers at the bases of conduits, we surmise that compound drops would have been widely distributed within the subvolcanic plumbing system. They were therefore available to be erupted in the coeval lavas. Upon pressure drop during eruption, a proportion of the metal originally bonded to sulfide became incorporated into the vapor phase and subsequently into aerosol. The next section considers how efficient that process may have been with regard to the transfer of Ni from sulfide melt into volcanic gas.

Nickel Concentrations in the Volcanic Gases

The model proposed here requires that Ni be transferred from the sulfide liquid into the gas phase and hence into volcanic aerosols during eruption. Here we test this hypothesis using simple thermodynamic models (6) to estimate the equilibrium partitioning of Ni between silicate melt, sulfide melt, and a low-density volcanic vapor phase.

Ni is dissolved in the silicate melt as a NiO species, and enters sulfide melt as NiS. During magma degassing at low pressure, sulfide melt reacts with H_2O to produce H_2S. Ni in the sulfide melt can enter the vapor phase as three different species: NiS(g), NiCl(g), or $NiCl_2$(g). The transfer of Ni from the melt to the vapor phase can therefore be described through the following reactions (Rn = Reaction n):

$$R_0 \quad NiS_{(1)} = NiS_{(g)},$$

$$R_1 \quad NiS_{(1)} + 2\ HCl_{(g)} = NiCl_{2(g)} + H_2S_{(g)},$$

$$R_2 \quad NiS_{(1)} + HCl_{(g)} = NiCl_{(g)} + 0.5\ H_{2(g)} + 0.5\ S_{2(g)}.$$

Apart from temperature, according to R_0 the concentration of NiS(g) does not depend on any intensive parameters other than the activity of the NiS component in sulfide liquid. In sulfide-undersaturated systems the concentration of $NiS_{(g)}$ will be low; however, in the presence of magmatic Cl, R_1 and R_2 will dominate gaseous Ni concentrations. The fugacity of H_2S in R_1 is related to fO_2, fH_2O, and fS_2:

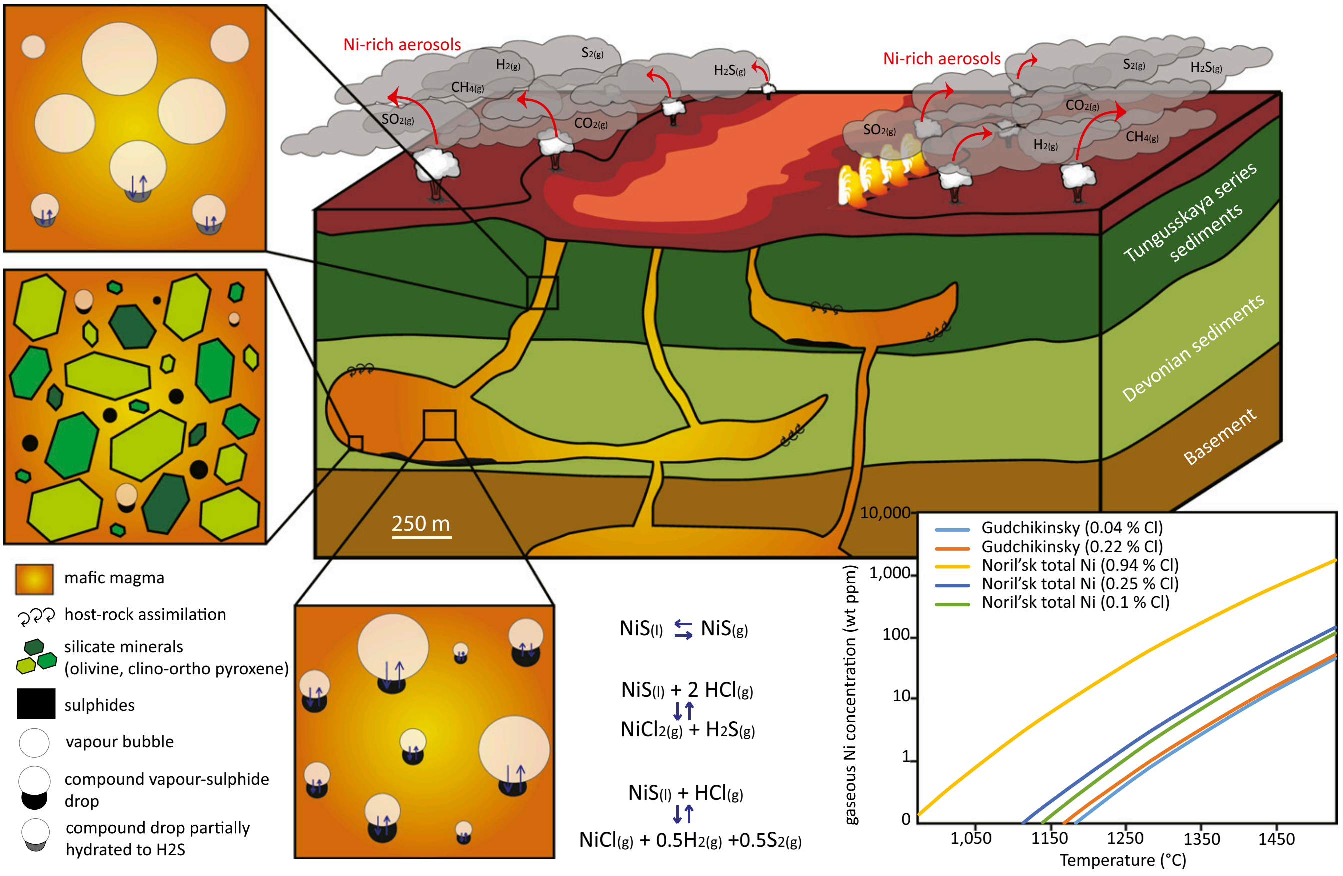

Fig. 4. Three-dimensional block diagram representing the processes described in this paper. (*Inset*) Results of the partition coefficient calculation for the reactions getting Ni from sulfide to vapor phase.

$$R_3 \quad H_2O_{(g)} + 0.5\ S_{2(g)} = H_2S_{(g)} + 0.5\ O_{2(g)}.$$

The fugacity of oxygen is assumed to be buffered externally at values close to that of the solid oxygen buffer fayalite + quartz + magnetite (FMQ). It is expressed as the difference between the value of logarithm of fO_2 of the system and that of the FMQ buffer (21) at a given temperature. This difference is written ΔFMQ; for the sulfide-undersaturated alkali picrites, ΔFMQ was set to -1.0 whereas for sulfide-saturated magmas in the Noril'sk intrusions ΔFMQ was set to 0.0. The fugacity of sulfur in a system containing both sulfide liquid and silicate melt is assumed to be buffered by the reaction

$$R_4 \quad FeO_{(melt)} + 0.5\ S_{2(g)} = FeS_{(l)} + 0.5\ O_{2(g)}.$$

Here the activities of FeO and FeS in the silicate melt and sulfide liquid are considered to be approximately equal to their mole fractions. It is noteworthy that due to the interplay of fO_2 and fS_2 in R_3 and R_4, the value of ΔFMQ has little net effect on the concentrations of gaseous Ni species. The fugacity of H_2 is assumed to be governed by the dissociation of water vapor:

$$R_5 \quad H_2O_{(g)} = H_{2(g)} + 0.5\ O_{2(g)}.$$

The fugacity of Cl was estimated as a function of the concentration of Cl in silicate melt (22) and it was assumed that all Cl in the vapor phase exists in the form of HCl at low pressure (22). Fugacities of gas species are assumed to be equal to mole fractions at 1 bar and magmatic temperatures. All thermochemical data were obtained from the JANAF tables online (23). In the present example fH_2O was set to 0.75, allowing for the presence of other gaseous components such as H_2S, SO_2, and CO_2 in the gas. Allowing fH_2O to approach 1 has little effect on gaseous Ni concentrations. The composition of the sulfide melt was set to $X_{NiS} = 0.5$ and $X_{FeS} = 0.5$. For nominally sulfide-undersaturated conditions (e.g., Gudchikinsky alkali picrite) the activity of $NiS_{(l)}$ was set to 0.2. Activity of FeO in the silicate melt was set at 0.12.

The concentration of Ni in volcanic gas predicted by this calculation (Fig. 4, *Inset*) is highly sensitive to temperature and depends exponentially on the availability of HCl and H_2S species in the gas phase. If basaltic magmas are not highly enriched in Cl, the dominant gaseous species of Ni at equilibrium with a sulfide liquid will be $NiS_{(g)}$. Sulfide-undersaturated magmas will have lower NiS(g) fugacities. At moderate magmatic Cl concentrations, the $NiCl_{2(g)}$ species dominates the total Ni budget in the volcanic gas. The Siberian Traps were exceptionally enriched in Cl (24, 25) at two distinct stages in their evolution. Early sulfide-undersaturated picrites were Cl-rich because their pyroxenitic mantle source incorporated ancient subducted crust (25). The main overlying stack of tholeiitic basalts and alkaline picrites contained far less Cl (24); however, assimilation of upper crustal sedimentary rocks including evaporites caused massive Cl enrichment in the magmas associated with the Ni deposits of the Noril'sk I–Maslovsky and associated ore-bearing intrusions (25) Although existing data documenting Cl concentrations in SLIP magmas are limited in number, it is clear that some of the magmas contained highly unusually enriched Cl concentrations, and that the only episode in which magmas were simultaneously saturated with immiscible NiS liquid and highly enriched in Cl was the intrusion of the ore-bearing intrusions. Fig. 4 (*Inset*) shows estimated total Ni concentrations as functions of eruptive temperature in volcanic gases for early sulfide-undersaturated alkali picrites and upper and lower limits for gases at equilibrium with Cl-rich sulfide-saturated magmas of the mineralized Noril'sk I–Maslovsky intrusion (25). Also shown is the estimated total Ni content of a vapor emanating from a hypothetical sulfide-saturated magma with the highest recorded Cl content in the SLIP [0.94 wt %; Bratsk dolerite sill (26)]. It is difficult to assign a temperature of emplacement to the magmas in the ore-bearing intrusions, but modeling of the conditions of magma contamination and ore formation suggest a range between 1,400 and 1,100 °C (27). Within the limited number of data available we cannot point to an individual sample exemplifying all of the required characteristics of sulfide saturation, high Cl content, and high emplacement temperature, but we contend that at least some of the ore-related intrusive rocks likely contained as much Cl as the highest values recorded in other subvolcanic sills while remaining near the temperature of the hot parental magmas. We conclude that the only magmas in the SLIP that could be expected to generate large emissions of Ni-rich aerosols were the highly contaminated sulfide-saturated magmas that generated the Noril'sk Ni–sulfide ore deposits and coeval basalts.

High a_{NiS} (i.e., saturation with large volumes of Ni-rich magmatic sulfide) and high f_{HCl} maximize the possible Ni emissions; these are two features of the Siberian traps that are not shared by other LIPs. The flotation of NiS liquid into erupting lavas through the bubble-attachment mechanism might have permitted a few major pulses of Ni emission far exceeding what would normally be emitted from sulfide-undersaturated basalts containing ~100 ppm Ni.

Conclusions

The Noril'sk Ni–Cu–platinum-group element (PGE) deposits are the only known occurrences of ore formation in high-level intrusions under subaerial lavas, and the only known example of a flood basalt-associated magmatic sulfide system that was shallow enough to degas during its formation. This peculiar setting, coupled with the extensive availability of assimilated volatiles from country-rock evaporites, would engender rapid pressure fluctuations accompanying explosive eruptions, favorable to degassing of the sulfides and host silicate magma. This degassing, combined with the observed association between nickel-rich sulfide globules and former vapor bubbles, and the interpretation of the flotation mechanism (19) as a viable way to float sulfides up within the magmatic conduit, would engender the release of large volumes of nickel-rich volcanic gases and aerosols into the atmosphere, in a form that allows it to be transported long distances, playing an important role in the onset of the Permian–Triassic mass extinction.

Methods

A high-resolution 3D X-ray scan of a representative sample was collected using the XRADIA XRM high-resolution 3D X-ray microscope system at the Australian Resources Research Centre, Perth, Australia, following a specific analytical technique and data processing protocol (28). Parameters used for the analysis were a voltage of 140 kV, a power of 10 W, and a pixel size of 10.81 μm. Per 360° rotation of the sample, 1,600 projections were collected.

The Maia detector array on the XRF microscopy beamline, at the Australian Synchrotron in Melbourne, allows the production of elemental maps with ~10-ppm detection limits and a resolution of up to 2 μm (29, 30).

ACKNOWLEDGMENTS. We thank Nadya Krivolutskaya for giving us access to some of the samples used in this study. We are also grateful to Michael Verrall for his help in mineral characterization. The three-elemental maps presented in Figs. 2 and 3 were collected using the Maia Detector on the X-ray fluorescence microscopy beamline on the Australian Synchrotron in Clayton, Victoria, Australia. and we acknowledge the assistance of Daryl Howard, David Paterson, Martin De Jonge, and Kathryn Spiers. We acknowledge financial support for this facility from the Science and Industry Endowment Fund.

1. Cao C, et al. (2009) Biogeochemical evidence for euxinic oceans and ecological disturbance presaging the end-Permian mass extinction event. *Earth Planet Sci Lett* 281(3-4): 188–201.
2. Fedorenko V, Czamanske G, Zen'ko T, Budahn J, Siems D (2000) Field and geochemical studies of the melilite-bearing Arydzhangsky Suite, and an overall perspective on the Siberian alkaline-ultramafic flood-volcanic rocks. *Int Geol Rev* 42(9):769–804.

3. Burgess SD, Bowring SA (2015) High-precision geochronology confirms voluminous magmatism before, during, and after Earth's most severe extinction. *Sci Adv* 1(7): e1500470.
4. Rothman DH, et al. (2014) Methanogenic burst in the end-Permian carbon cycle. *Proc Natl Acad Sci USA* 111(15):5462–5467.
5. Allard P, et al. (2000) Acid gas and metal emission rates during long-lived basalt degassing at Stromboli volcano. *Geophys Res Lett* 27(8):1207–1210.
6. Symonds RB, Reed MH (1993) Calculation of multicomponent chemical equilibria in gas-solid-liquid systems: Calculation methods, thermochemical data, and applications to studies of high-temperature volcanic gases with examples from Mt. St. Helens. *Am J Sci* 293(8):758–864.
7. Seinfeld JH, Pandis SN (2006) *Atmospheric Chemistry and Physics: From Air Pollution to Climate Change* (John Wiley & Sons, Hoboken, NJ), 2nd Ed, pp 791–792.
8. Allen A, et al. (2006) Sources, size distribution, and downwind grounding of aerosols from Mount Etna. *J Geophys Res Atmos*, 10.1029/2005JD006015.
9. Martin R, et al. (2008) Composition-resolved size distributions of volcanic aerosols in the Mt. Etna plumes. *J Geophys Res Atmos*, 10.1029/2007JD009648.
10. Rose W, Chuan R, Cadle R, Woods D (1980) Small particles in volcanic eruption clouds. *Am J Sci* 280(8):671–696.
11. Allen AG, Baxter PJ, Ottley CJ (2000) Gas and particle emissions from Soufrière Hills Volcano, Montserrat, West Indies: Characterization and health hazard assessment. *Bull Volcanol* 62(1):8–19.
12. Calabrese S, et al. (2011) Atmospheric sources and sinks of volcanogenic elements in a basaltic volcano (Etna, Italy). *Geochim Cosmochim Acta* 75(23):7401–7425.
13. Moune S, Gauthier P-J, Delmelle P (2010) Trace elements in the particulate phase of the plume of Masaya Volcano, Nicaragua. *J Volcanol Geotherm Res* 193(3):232–244.
14. Mather TA, Pyle DM, Oppenheimer C (2004) Tropospheric volcanic aerosol. *Volcanism and the Earth's Atmosphere*, eds Robock A, Oppenheimer C (American Geophysical Union, Washington, DC), pp 189–212.
15. Schäfer K, et al. (2011) Influences of the 2010 Eyjafjallajökull volcanic plume on air quality in the northern Alpine region. *Atmos Chem Phys Discuss* 11(3):9083–9132.
16. Malitch KN, Latypov RM, Badanina IY, Sluzhenikin SF (2014) Insights into ore genesis of Ni-Cu-PGE sulfide deposits of the Noril'sk Province (Russia): Evidence from copper and sulfur isotopes. *Lithos* 204:172–187.
17. Likhachev A (1994) Ore-bearing intrusions of the Noril'sk region. *Proceedings of the Sudbury-Norilsk Symposium*, eds Lightfoot PC, Naldrett AJ (Ontario Geological Survey, Sudbury, ON, Canada), pp 185–202.
18. Barnes S-J, Makovicky E, Makovicky M, Rose-Hansen J, Karup-Moller S (1997) Partition coefficients for Ni, Cu, Pd, Pt, Rh, and Ir between monosulfide solid solution and sulfide liquid and the formation of compositionally zoned Ni-Cu sulfide bodies by fractional crystallization of sulfide liquid. *Can J Earth Sci* 34(4):366–374.
19. Mungall JE, Brenan JM, Godel B, Barnes S, Gaillard F (2015) Transport of metals and sulphur in magmas by flotation of sulphide melt on vapour bubbles. *Nat Geosci* 8(3): 216–219.
20. Anderson AT, Jr, Swihart GH, Artioli G, Geiger CA (1984) Segregation vesicles, gas filter-pressing, and igneous differentiation. *J Geol* 92(1):55–72.
21. O'Neill HS (1987) Quartz-fayalite-iron and quartz-fayalite-magnetite equilibria and the free energy of formation of fayalite (Fe 2 SiO 4) and magnetite (Fe 3 O 4). *Am Mineral* 72(1-2):67–75.
22. Shinohara H (2009) A missing link between volcanic degassing and experimental studies on chloride partitioning. *Chem Geol* 263(1):51–59.
23. Chase MW (1996) NIST-JANAF thermochemical tables for oxygen fluorides. *J Phys Chem Ref Data* 25(2):551–603.
24. Sibik S, Edmonds M, Maclennan J, Svensen H (2015) Magmas erupted during the main pulse of Siberian Traps volcanism were volatile-poor. *J Petrol* 56(11):2089–2116.
25. Sobolev AV, Arndt NT, Krivolutskaya NA, Kuzmin DV, Sobolev SV (2015) The origin of gases that caused the Permian-Triassic extinction. *Volcanism and Global Environmental Change*, ed Schmidt A, Frustard KE, Elking-Tantto L (Cambridge Univ Press, Cambridge, UK), pp 147–163.
26. Black BA, Elkins-Tanton LT, Rowe MC, Peate IU (2012) Magnitude and consequences of volatile release from the Siberian Traps. *Earth Planet Sci Lett* 317:363–373.
27. Mungall JE (2014) Geochemistry of magmatic ore deposits. *Treatise on Geochemistry: Geochemistry of Mineral Deposits* (Elsevier, Amsterdam), 2nd Ed Vol 13, pp 195–218.
28. Godel B (2013) High-resolution X-ray computed tomography and its application to ore deposits: From data acquisition to quantitative three-dimensional measurements with case studies from Ni-Cu-PGE deposits. *Econ Geol* 108(8):2005–2019.
29. Fisher LA, et al. (2015) Quantified, multi-scale X-ray fluorescence element mapping using the Maia detector array: Application to mineral deposit studies. *Miner Depos* 50(6):665–674.
30. Ryan CG, et al. (2010) Elemental X-ray imaging using the Maia detector array: The benefits and challenges of large solid-angle. *Nucl Instrum Methods Phys Res A* 619(1-3):37–43.